Pakistan Journal of Medical & Cardiological Review
https://pakjmcr.com/index.php/1/about
Online ISSN 3007-2387
Print ISSN 3007-2379

# Advanced CNN-Based Brain Tumor Detection and Segmentation Using MATLAB: A Diagnostic Accuracy Study

**Hira Yousaf**
Department of Radiology and Imaging Technology, The University of Faisalabad, Pakistan

**Hamza Rehman Qureshi**
Department of Radiology, ATLAS Diagnosis Service, Pakistan

**Amna Noor**
Faculty of Allied Health Sciences, Superior University Lahore, Pakistan

**Ayesha Hameed**
Department of Radiology and Imaging Technology, Green International University Lahore, Pakistan

**Syed Sami Ahmad Samar Bukhari***
Faculty of Allied Health Sciences, Superior University Lahore, Pakistan
Email: samibukhari79@gmail.com

**Raqiba Munir**
Faculty of Allied Health Sciences, Superior University Lahore, Pakistan

**Author Details**

**Keywords:** MATLAB, Brain Tumor, Tumor Detection in MATLAB.

**Received on 25 Dec 2025**
**Accepted on 20 Feb 2026**
**Published on 03 Feb 2026**

**Corresponding E-mail & Author*:**

**Syed Sami Ahmad Samar Bukhari***
Faculty of Allied Health Sciences, Superior University Lahore, Pakistan
Email: samibukhari79@gmail.com

**Abstract**

The brain tumor is intracranial mass made up by abnormal growth of tissue in the brain or around the brain. The new CNN technique in MATLAB can be used to detect the brain tumors more precisely. The study objective was to get the easily diagnose of the Tumor and to get the Segmentation of the Tumor using MATLAB. This analytical study was conducted in MATLAB which is a software. The sample size of 100 was estimated by using 95% confidence level with 5% margin of error and taking an expected percentage of Brain Tumor as 99%. The data consisted of 100 patients. The data was gathered from both males and females. There was total 97 patients, out of which around 67 were males and around 33 were female. According to the previous method diagnosis, there were around 42 patients (42%) that had the benign indication of Brain Tumor and around 58 patients (58%) that malignant indication of Brain Tumor. According to MATLAB results, around 51 patients (51%) had benign type of Brain Tumor and around 49 patients (49%) had malignant type of cervical lymphadenopathy. The main analytical statistics proved the diagnostic odd ratio statistics to be around 97% with the sensitivity of MATLAB in differentiating between benign and malignant Brain Tumor was around 99% with

the specificity around 98% with disease prevalence to be around 96% with positive and negative predictive values to be around 99% and 1%. Our experimental results demonstrated that both models enhance the prediction performance of diagnosis of brain tumors. We achieved 97.8% and 100% prediction accuracy for dataset 1 and dataset 2, respectively outperforming previous studies found in the literature. Therefore, we believe that our proposed methods are outstanding candidates for brain tumor detection.

## Introduction

An unusual mass of tissue in which some cells multiply and grow uncontrollably is called brain tumor. It starts growing inside the skull and interpose with the regular functioning of the brain. It needs to be detected at an early stage using MRI or CT scanned images when it is as small as possible because the tumor can possibly result to cancer. Human body is made up of several type of cells [1]. Brain is a highly specialized and sensitive organ of human body. Tumor is defined as the abnormal growth of cells. Brain tumor is an abnormal mass of tissue in which cells grow and multiply uncontrollably, seemingly unchecked by the mechanisms that control normal cells. The symptoms of brain tumor depend on the tumor size, type and location [2]. Brain tumor is a very harmful disease for human being. The brain tumor is intracranial mass made up by abnormal growth of tissue in the brain or around the brain. Brain tumor disease refers to the presence of abnormal growths or tumors in the brain [5].

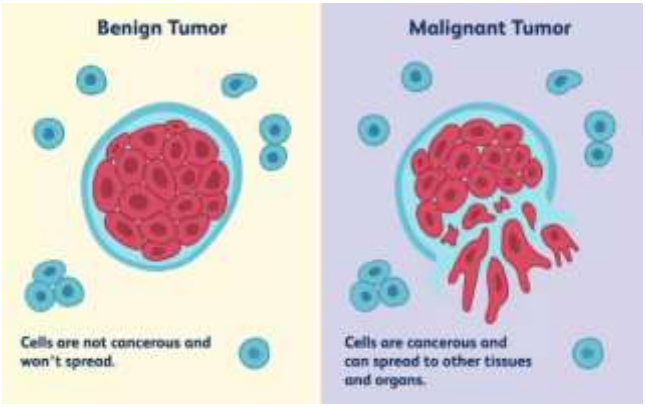


Fig 1. Benign and Malignant Brain Tumor

The malignant tumors it spread rapidly entering other tissues of the brain therefore, worsening condition patients are loosed brain tumors can originate from brain tissue (primary brain tumors) or spread to the brain from other parts of the body (secondary or metastatic brain tumors). The exact causes of brain tumors are often unknown, but certain risk factors have been identified, Such as Genetic factors, exposure to radiation or family history [6].

MATLAB is a high-level technical language and interactive environment for data analysis and mathematical computing functions such as: signal processing, optimization, partial differential equation solving, etc. It provides interactive tools including: threshold, correlation, Fourier analysis, filtering, basic statistics, curve fitting, matrix analysis, 2D and 3D plotting functions. The operations for image processing allowed us to perform noise reduction and image enhancement, image transforms, color map manipulation, color space conversions, region-of interest processing, and geometric operation. The toolbox functions implemented in the open MATLAB language can be used to develop the customized algorithms [7].

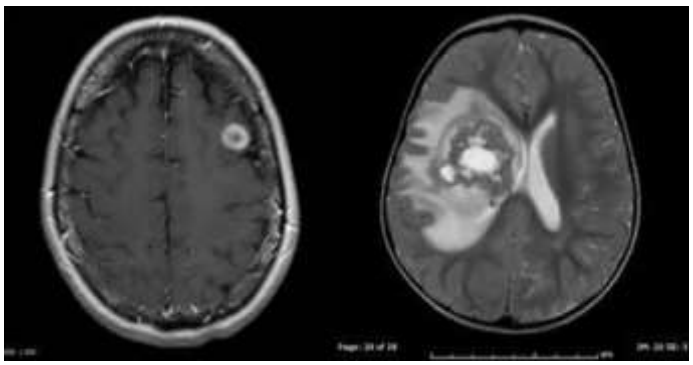

Fig 2. Benign and malignant tumors on MRI

The brain tumor detection can be done through MRI Imaging [7]. In image processing and image enhancement tools are used for medical imaging processing to improve the quality of the image The contrast adjustment and threshold techniques are used for highlighting the features of MRI images. The Edge detection, Histogram, Segmentation and Morphological operations play a vital re for classification and detection of the brain tumors [8].

The various steps of MR imaging like; preprocessing, feature extraction, segmentation, post-processing, etc.[7] which is used for finding the tumor area of MRI-images. The figure-1 show basic structure of feature extraction through Digital image processing.

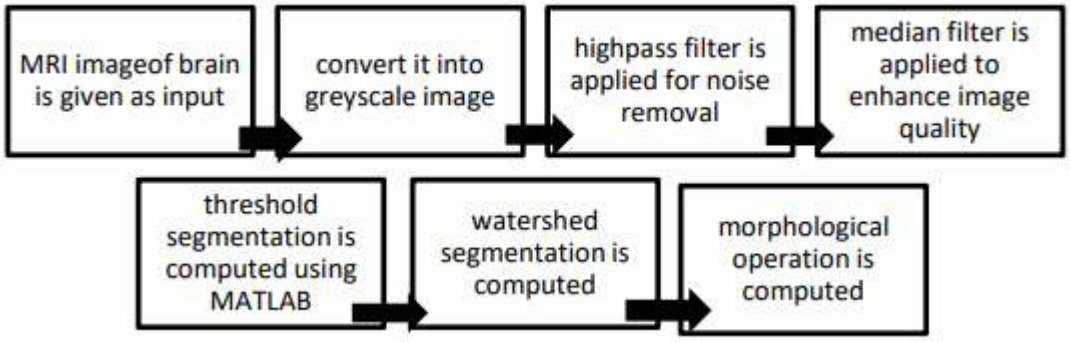


Figure 3. System Level Block Diagram

Grayscale image is preferred format for image processing because gray scale images are much less complex and one can talk in detail about contrast, brightness, and edges without considering colors [12]. Colors are much more complex since they are composed of three channels that are why image is converted into grayscale before further processing in image segmentation [9].

Artificial Neural Networks (ANNs) are mathematical tools to approximate functions that depend on large number of inputs [10]. ANNs consist of interconnected mathematical functions, 'neurons', which exchange messages between each other. Connected neurons have 'weights', that adjust adaptively with respect to given inputs and outputs so that the entire network can learn the input and output patterns and suitably approximate the given pattern. ANN architecture can be classified into three categories based on its connection structures: Feedforward, Feedback (recurrent) and Hybrid [11]. Feedforward networks are further classified into Multilayer Perceptron (MLP), Counter-propagation Networks, Cerebellar Model Articulation Controller, Radial Basis Function (RBF) and Self Organized Mapping (SOM) networks. Our study objective was to facilitate accurate and efficient brain tumor diagnosis using image processing and segmentation techniques implemented in MATLAB.

## MATERIALS AND METHODS

### Study Design and Setting

This study was conducted as a descriptive analytical study. The research was carried out using data obtained from the Harvard Medical website, which provides clinically relevant medical imaging data for research and educational purposes.

#### Duration of Study

The total duration of the study was four months, commencing after the formal approval of the research synopsis.

### Sample Size and Selection Criteria

The sample size was determined using an appropriate statistical formula, supported by reference to a previously published study. Patients were selected based on predefined inclusion and exclusion criteria.

**Inclusion criteria** included patients with a history and clinical manifestations suggestive of a brain tumor, as well as patients with a provisional or confirmed diagnosis of a brain tumor.

**Exclusion criteria** included patients with any known contraindications to magnetic resonance imaging (MRI), such as implanted metallic devices or other MRI-incompatible conditions.

### Equipment and Data Sources

The primary resources utilized in this study included the Harvard Medical website for medical imaging data and the MATLAB application for image processing and analysis. MATLAB's Image Processing Toolbox and other relevant computational tools were employed to facilitate accurate image segmentation and analysis.

#### Scanning Technique and Image Processing

Magnetic Resonance Imaging (MRI) and Computed Tomography (CT) scans were used for the detection of brain tumors, with MRI serving as the preferred imaging modality due to its superior soft tissue contrast and sensitivity. MRI images were processed using MATLAB to enhance image quality and facilitate tumor detection. The preprocessing steps included noise and artifact removal, followed by segmentation of the brain from the background. Subsequently, tumor regions were segmented from normal brain tissue. Feature extraction was performed on the segmented images to differentiate between normal and tumor tissues. The accuracy of segmentation and analysis was validated by comparing the results with ground truth data or established reference standards.

### Data Collection Procedure

MRI scans of patients with and without brain tumors were obtained and systematically processed using MATLAB. The extracted imaging data were used to train and validate a machine learning model for brain tumor detection. Various computational tools were utilized, including MATLAB's Image Processing Toolbox, the Medical Image Computing and Computer-Assisted Intervention (MICCAI) toolbox, and the Insight Segmentation and Registration Toolkit (ITK). The primary variable assessed was the presence or absence of a brain tumor. Additional variables included tumor size, location, and type, as well as patient demographic characteristics such as age, gender, and relevant medical history.

### Data Analysis Procedure

Statistical analysis was performed using SPSS version 24.0 for Windows. Categorical variables were expressed as absolute frequencies (n) and percentages (%), while continuous variables were presented as mean ± standard deviation for parametric data or median with percentiles for nonparametric data. A p-value of less than 0.05 was considered statistically significant. Diagnostic performance measures, including odds

ratios (OR), sensitivity, specificity, positive predictive value (PPV), negative predictive value (NPV), and positive and negative likelihood ratios, were calculated.

### Ethical Considerations

The study was conducted in accordance with the ethical guidelines and regulations set by the Ethical Committee of Superior University, Lahore. Written informed consent was obtained from all participants prior to data inclusion. Participant confidentiality and anonymity were strictly maintained throughout the study. All collected data were kept secure and used solely for research purposes. Participants were informed that there were no known risks associated with the study and that participation was entirely voluntary. They were also informed of their right to withdraw from the study at any time without penalty. No identifying information was disclosed in any publication resulting from this research.

## RESULTS

In this study, two different data sets are used. The first one (referred to as dataset 1) The data is collected from Harvard medical Website, during 2020 to 2023. This data set contains a total of 3064 T1- weighted contrast MRI slices from 233 patients diagnosed with one of the three brain tumors, including meningioma, glioma, and pituitary (as shown in Fig. 3). The MRI images used in this data set have three different views including axial, coronal, and sagittal.

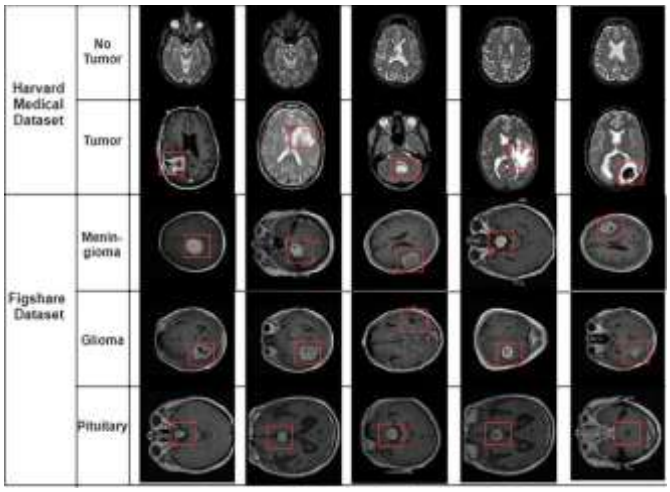


The second dataset (referred to as dataset 2) is collected by the Harvard repository. The dataset includes a total of 152 T1 and T2-weighted contrast MRI slices. Among them, 71 slices are healthy images that do not contain any tumor, and a total of 81 are abnormal images containing a tumor. The abnormal brain slices have five different types of tumors, including Glioma, Metastatic adenocarcinoma, Metastatic bronchogenic carcinoma, Meningioma, and Sarcoma (as shown in 3).

Table 2, Table 1 include detail information of these two data sets.

**Table 1**

**Number of MRI slices in dataset 2.**

| Brain | Tumor Class | Number of Slices |
|---|---|---|
| Normal | Normal Image | 71 |
| Abnormal | Glioma | 29 |
| | Metastatic audenocarcinoma | 8 |

| | | |
|---|---|---|
| | Metastatic bronchogenic carcinoma | 12 |
| | Meningioma | 16 |
| | Sarcoma | 16 |
| Total | | 152 |

**Table 2**

**Number of MRI slices in dataset 1.**

| Tumor Class | Number of Patients | Number of MR Slices |
|---|---|---|
| Meningioma | 82 | 708 |
| Glioma | 91 | 1426 |
| Pituitary | 60 | 930 |
| Total | 233 | 3064 |

We employ several preprocessing techniques before feeding the images into our classifiers. For instance, all the MRI images in the Figshare dataset are in.mat type (defined in Matlab). Hence, to read the image, we require to expand the dimension of the image. After that, we transform all the images into NumPy arrays (available in python) so that our model can take up less space. Before splitting the dataset, we have shuffled the data so that our model can train on unordered data. After shuffling the data, we divide the dataset into three sections including train, test, and validation. Approximately 70% of the data is used for training, and a further 30% is used for validation and testing purposes (see Table 4).

**Table 4**

**MRI slices distribution for training validation and testing purposes.**

| Dataset | Brain Tumor Type | Training | Validation | Testing |
|---|---|---|---|---|
| Harvard Medical | Normal | 357 | 42 | 14 |
| | Abnormal | 406 | 49 | 16 |
| Figshare | Meningioma | 502 | 56 | 150 |
| | Glioma | 1032 | 115 | 279 |
| | Pituitary | 674 | 75 | 181 |

On the other hand, all the MRI images in the Harvard Medical dataset are in.GIF type. To process the dataset, we have converted the MRI images to.JPEG type. To reduce the image's dimensionality, we down-size the original image from $256 \times 256 \times 1$ to $128 \times 128 \times 3$. We replicate the pixel intensity value three times to create three channels according to the pre-trained VGG16 architecture input size. As a result, the number of images increased from 152 to 884 after performing data augmentation. Additionally, we have used 70% of the data to train the model, and a further 30% of the data were used to validate and test the proposed method. (see Table 4).

**Table 3**

**Data augmentation strategy used in this study.**

| Serial | Parameter | Value |
|---|---|---|
| 1 | shear range | 0.2 |
| 2 | zoom range | 0.2 |

| | | |
|---|---|---|
| 3 | rotation | 90 |
| 4 | width shift range | 0.1 |
| 5 | height shift range | 0.1 |
| 6 | vertical_flip | True |
| 7 | horizontal_flip | True |

**Proposed 23-layers CNN architecture**

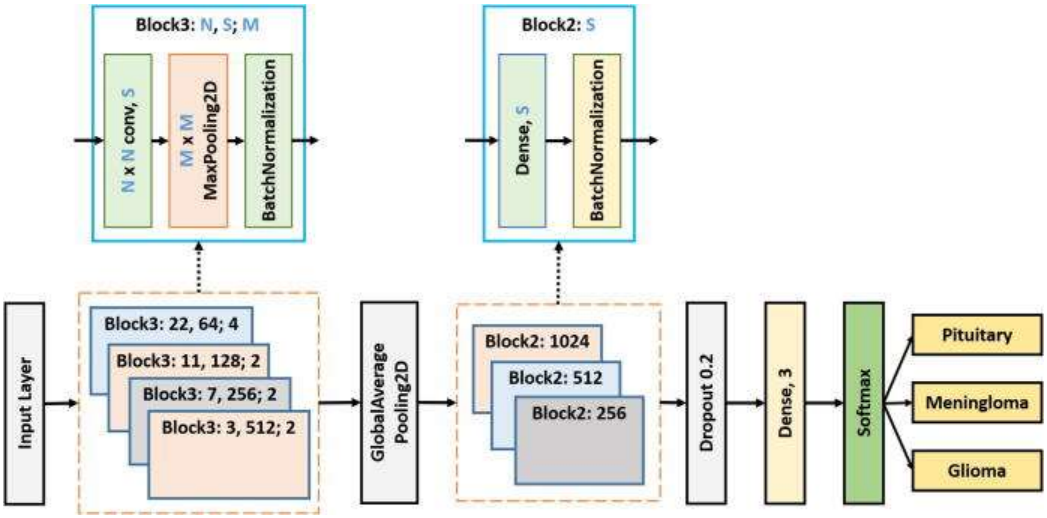


One of the predominant building blocks of the CNN model is the convolutional layer. It is a mathematical method that performs a dot product between two matrices to construct a transformed feature map. One matrix relates to the kernel, while the other presents the pixel intensity values of the original image. The kernel is used to move vertically and horizontally over the original image to extract properties such as borders, corners, shapes, etc.

$$C(h,d) = (k * f)(h,d) = \sum_i \sum_j k(h-i, d-j) f(i,j)$$

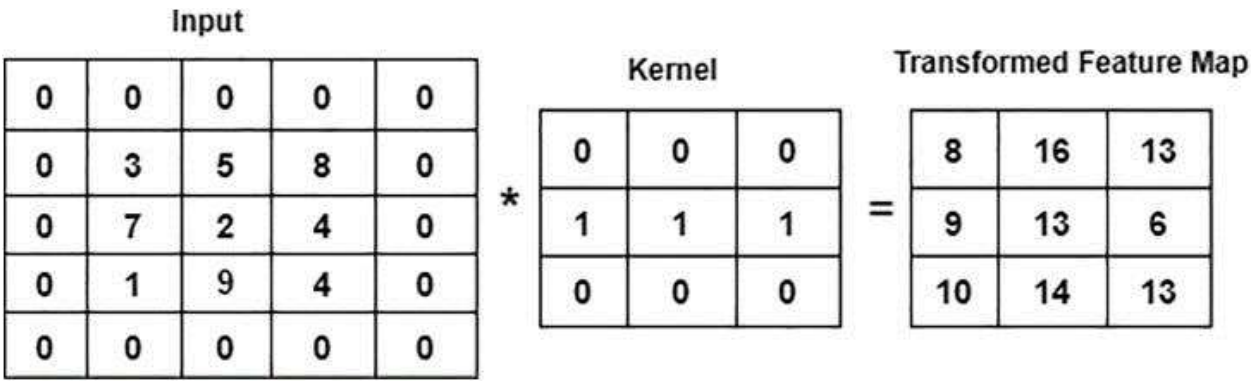


As an activation function, we use the Rectified Linear Unit (ReLU) which performs non-linear operations within the convolutional layer. The RelU activation function helps to solve the gradient vanishing problem using the backpropagation process. The RelU is defined as follows:

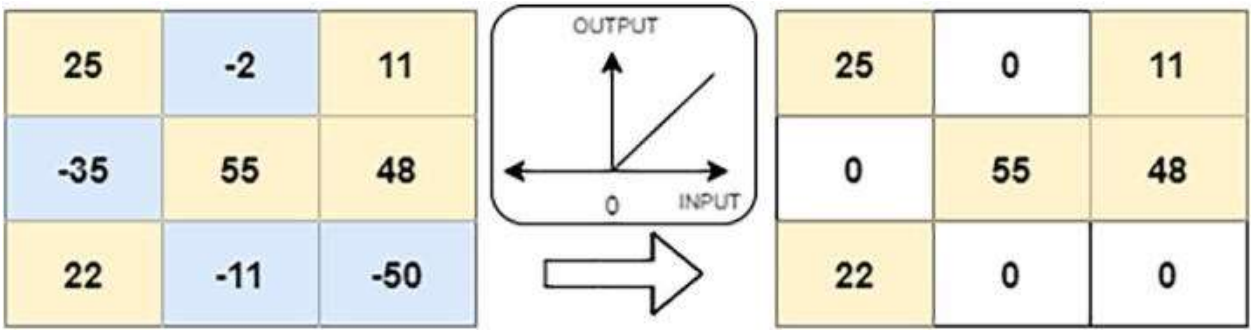


**Training and parameter optimization :**

For Study I (using dataset 1), Fig. 9 demonstrates both training and validation steps for the "23-layers CNN" architecture. The hyper-parameter optimization used for this training is presented in Table 5. As our loss function, we select sparse categorical cross-entropy. We also study different batch-sized optimizers to train the model. Among them, the Adam optimizer with batch size 32 obtained the best performance. We observe that the optimal convergence for the model depends on the initial learning rate of alpha. We have to select alpha very carefully because CNN does not converge well if alpha is very high. If alpha is very small, then CNN will take more time to converge. Here we select the alpha as 0.0001 to avoid these issues.

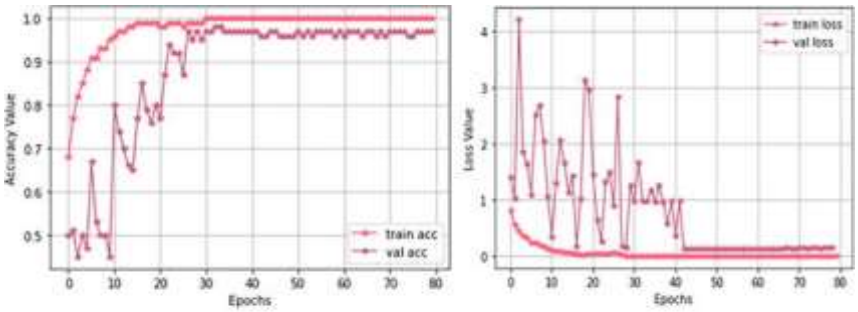


(a) (b)

**Table 5**

**Optimization of Hyper-Parameters for Study I and Study II.**

| Model | Hyper-parameters | setting |
|---|---|---|
| CNN | Loss function | sparse_categorical _crossentropy |
| | Optimizer function | adam |
| | Metrics | accuracy |
| | Epochs | 80 |
| | Batch_size | 32 |
| | Learning_rate | 0.0001 |
| CNN- Pretrained Model | Loss function | categorical _crossentropy |
| | Optimizer function | adam |
| | Metrics | accuracy |
| | Epochs | 40 |
| | Batch_size | 10 |
| | Learning_rate | 0.0001 |

For each epoch, Fig. 9(a) shows both training and validation progress. After the 29th epoch, the CNN model achieves 100% prediction accuracy with overall validation accuracy of 97.0%. Considering the consistency of the results (as shown in this figure), we can conclude that the "23-layers CNN" architecture successfully avoids the overfitting problem. Fig. 9(b) shows that the loss value decreases, and right after the 29th epoch, it hits zero for the training phase. Due to the limited batch size, some fluctuations occurred in the curve for the validation process. However the instability vanished after the 43rd epoch, and the loss curve approaches to zero.

The confusion matrix and the ROC curve for the Fig share data set are given in Fig. 10. In the Fig share data set, a "23-layers CNN" architecture was used for the prediction purpose. It can be observed from Fig. 10 that a total of 140, 270, and 180 MRI slices are correctly classified for meningioma, glioma, and pituitary tumors, respectively. While only 20 MRI slices are misclassified by the proposed architecture. The other performance metrics, including accuracy, precision, recall, FPR, TNR, and F1-score, are presented in Table 6. As shown in Table 6, the prediction accuracy of 96.7%, 97.2%, and 99.5% are achieved for meningioma, glioma, and pituitary tumors, respectively. Finally, the overall prediction accuracy achieved on the Fig share dataset is 97.8%. For the other performance metrics, we achieve an average precision of 96.5%, a recall of 96.4%, and an F1-score of 96.4%. The false-positive rate is approximately 0, and the true negative rate appears to be close to 1, which demonstrates that the "23-layers CNN" architecture can achieve excellent efficiency on the Fig share data set.

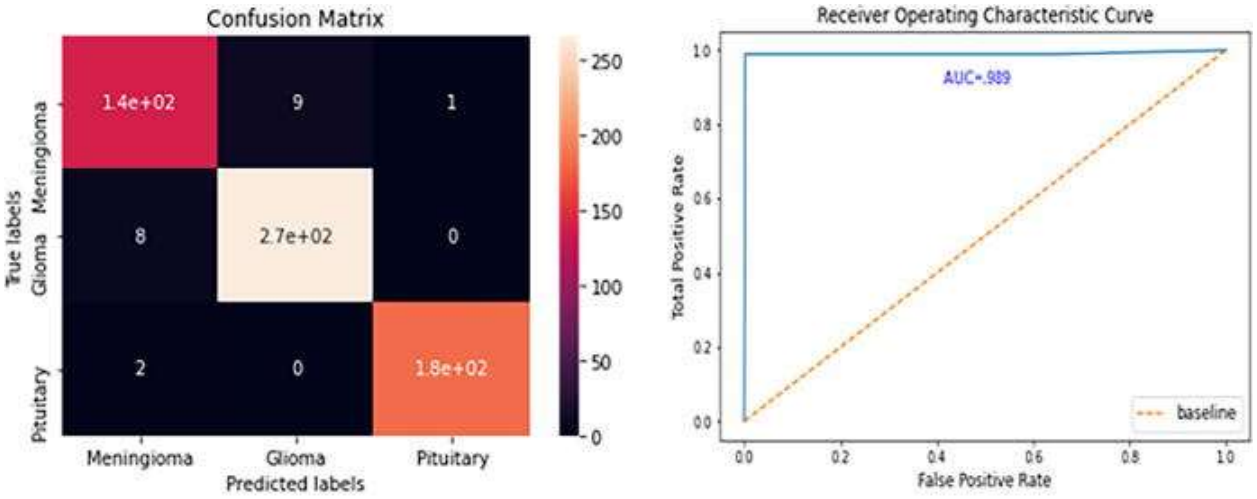


Table 6

**The results obtained using the CNN model on dataset1.**

| Metrics | Tumor class | TP | TN | FP | FN | Accuracy | Precision | Recall | FPR | TNR | F1-score |
|---|---|---|---|---|---|---|---|---|---|---|---|
| Figshare Dataset | Meningioma | 140 | 450 | 10 | 10 | 96.7% | 93.3% | 93.3% | 0.021 | 0.978 | 0.933 |

| | | | | | | | | | | |
|---|---|---|---|---|---|---|---|---|---|---|
| Glioma | 270 | 323 | 9 | 8 | 97.2% | 96.8% | 97.1% | 0.027 | 0.972 | 0.969 |
| Pituitary | 180 | 427 | 1 | 2 | 99.5% | 99.4% | 98.9% | 0.002 | 0.998 | 0.991 |
| Average Score | | | | | 97.8% | 96.5% | 96.4% | 0.016 | 0.983 | 0.964 |

From the ROC curve, we can observe that the area value is 0.989, which indicates the consistency and generality of our model.

We also apply our proposed "23 layers CNN" architecture to the Harvard Medical dataset. Here we achieved more than 85% training and validation accuracy on this dataset. However, the testing accuracy is less than 55%, indicating an overfitting issue occurred while training the model. Hence, to validate the system's performance and for solving the overfitting issue, the generalization technique was applied. As it was discussed earlier, to build this model, we combine VGG-16 model with some reflection of our proposed "23 layers CNN" architecture as shown in Fig. 8. In this way, we address the overfitting issue for the small dataset.

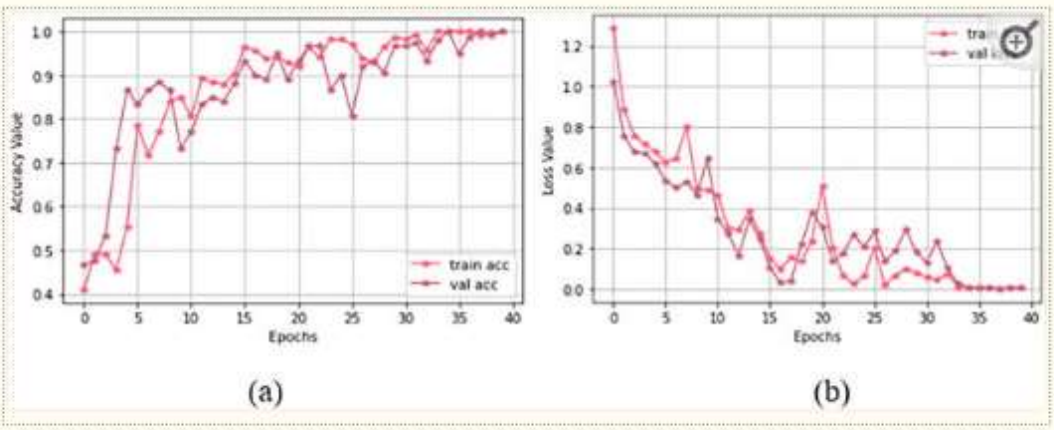


Fig. 14

Training progress for study I I: (a) accuracy value during training and validation process (preferred higher value), and (b) loss value during training and validation process (preferred lower value).

The confusion matrix and the ROC curves for dataset 1 are given in Fig. 13. In this dataset, a "Fine-tuned VGG16" architecture is tested on 30 images. Among them, 14 images contain no tumor, and 16 images include tumors. Interestingly, no MRI slices are misclassified by our proposed architecture. As shown in Fig. 13 all 14 and 16 MRI slices are correctly classified for normal and abnormal brain images, respectively. The other performance metrics are shown in Table 7. As shown in this table, we achieve an average accuracy of 100%, 100% precision, recall of 100%, and F1-score of 100%. The FNR is 0, and the TNR is 1 for dataset 2. From the ROC curve, we can also observe that the area under the curve value is 1, which indicates the model's consistency and generality.

Table 7

**The results obtained using the reflection of the proposed CNN model on dataset2.**

| Metrics | Tumor class | TP | TN | FP | FN | Accuracy | Precision | Recall | FPR | TNR | F1-score |
|---|---|---|---|---|---|---|---|---|---|---|---|
| Harvard Medical Dataset | No Tumor | 14 | 16 | 0 | 0 | 100% | 100% | 100% | 0 | 1 | 100 % |
| | Tumor | 16 | 14 | 0 | 0 | 100% | 100% | 100% | 0 | 1 | 100 % |
| | Average Score | | | | | 100% | 100% | 100% | 0 | 1 | 100 % |

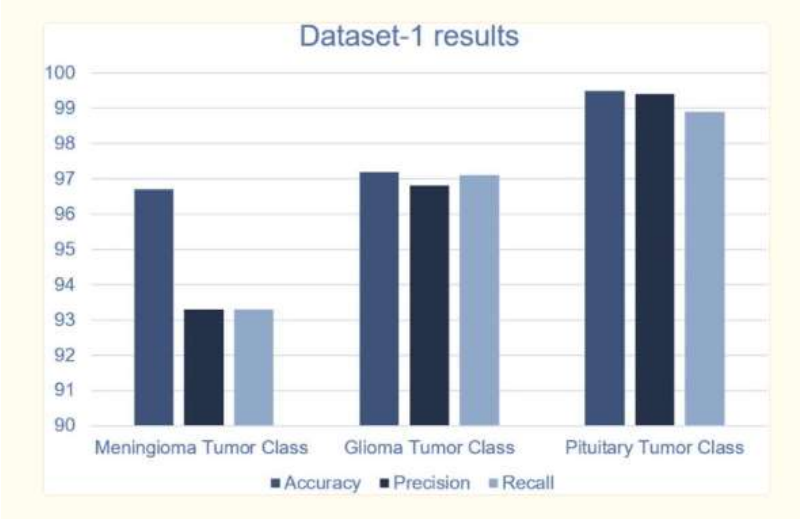


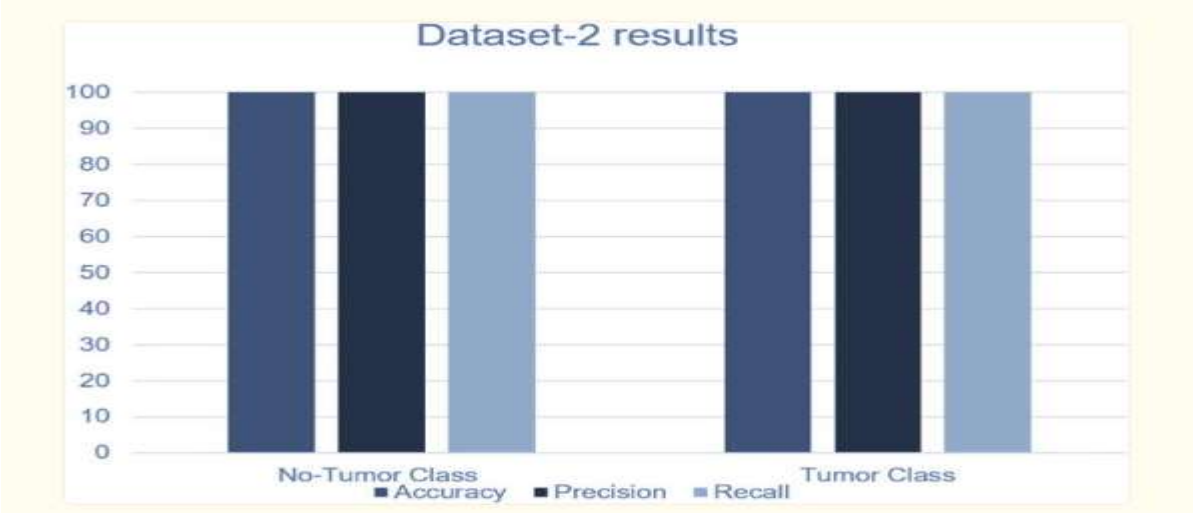

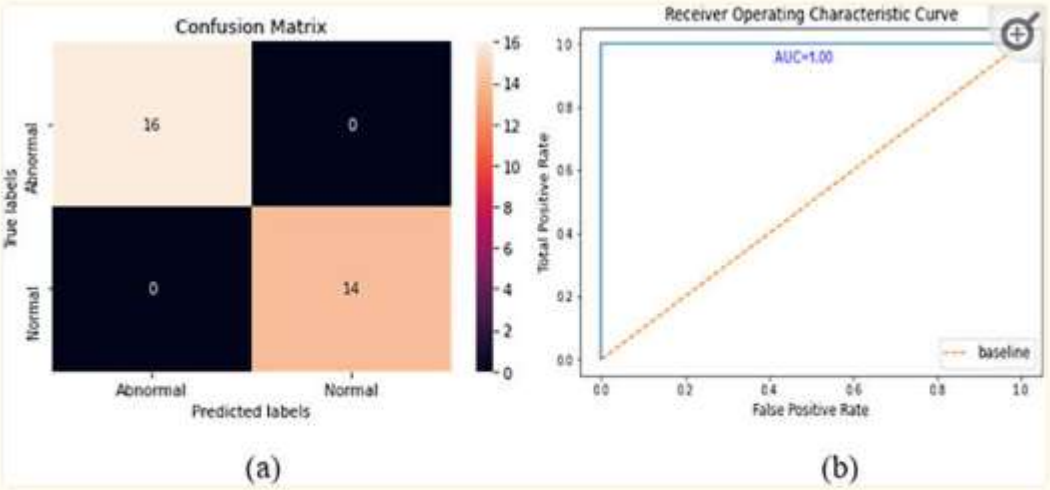


Fig. 13

Fine-tuned model's performance a) confusion matrix, b) ROC curve.

Table 9

Performance of different configurations on the Figshare dataset.

| Method | Loss Function | Activation Function | Accuracy on Figshare Dataset |
|---|---|---|---|
| 23-Layer CNN | Binary Cross Entropy | Sigmoid | 82% |
| 23-Layer CNN | Binary Cross Entropy | Tanh | 80% |
| 23-Layer CNN | Binary Cross Entropy | Softmax | 84% |
| 23-Layer CNN | Categorical Cross Entropy | Sigmoid | 89% |
| 23-Layer CNN | Categorical Cross Entropy | Tanh | 91% |
| 23-Layer CNN | Categorical Cross Entropy | Softmax | 92% |
| 23-Layer CNN | Sparse Categorical Cross Entropy | Sigmoid | 94% |
| 23-Layer CNN | Sparse Categorical Cross Entropy | Tanh | 95% |
| 23-Layer CNN | Sparse Categorical Cross Entropy | Softmax | 97.8% |

## DISCUSSION

For the Harvard Medical Dataset (dataset 2) and Fig share dataset (dataset 1), we have obtained 100% and 97.8% prediction accuracies, respectively. However, there are other advantages to our proposed model over the existing models found in the literature. For example, most of the methods require handcrafted feature extractor methods [13-14-15], which may not be very effective when dealing with a large number of images. While the "23-layers CNN" and "Fine-tuned CNN with VGG16" architectures are segmentation-free and do not require handcrafted features.

Previously, Anaraki et al., introduced GA with CNN to predict brain tumors [16]. GA, however, does not always demonstrate good precision when working with CNN. GA is also a computationally expensive model. In another research, Afshar et al., used CapsNets architecture to focus on both the tumor and its surrounding region [17-18-19]. However, defining two objects at the same time can compromise the results for

each individual problem despite their similarities. Swati and Sajjad et al., both applied the pre-trained VGG19 model to the Fig share dataset and obtained nearly the same performance [20-21]. However, they did not implement any dropout or regularization strategy to solve the issue of overfitting.

In another study, [22] segmented the tumor region using the active contour approach [23]. Active contour uses energy forces and limitations to extract the crucial pixels from an image for additional processing and interpretation. However, there are drawbacks that could occur while using active contouring in segmentation, such as getting stuck in local minima states while training or overlooking tiny details while minimizing the energy throughout the whole path of their contours. Momina et al. applied Mask RCNN along with the ResNet-50 model to locate the tumor region [24]. They have achieved 95% classification accuracy. However, more sophisticated object detection algorithms, such as the Yolo model and the Faster RCNN model, perform much better than the Mask RCNN. For instance, Eko et al. outperformed Mask RCNN by employing the Yolo model, which has a mAP rate of 80.12%, when segmenting the head and tail of fish [25].

Later on, Francisco et al., and Emrah et al. both used CNN model to obtain detection accuracy of more than 90% [26-27]. However, both models are computationally expensive and do not offer a method for system validation. Since a specific model may work well on one dataset while having detrimental effects on another, it is crucial to apply system validation techniques. In a similar study, Abiwinanda et al. proposed a CNN model to categorize tumor classes using only 700 MRI images from the Fig share dataset [28]. They also did not employ any data augmentation techniques in order to increase the amount of MRI images. As a result, they only achieved a classification accuracy of 84%, which is quite low compared to similar studies.

To classify the binary class, previous studies used an imbalance dataset [29]. We addressed this issue by using almost the same number of normal and abnormal brain MRI images. Besides, using the CNN model in the Figshare dataset, Sultan et al., achieved very promising results. However, there was still room for improvement by adding more layers into the network [30].

## Conclusion

This research introduces two deep learning models for identifying brain abnormalities as well as classifying different tumor grades, including meningioma, glioma, and pituitary. The application of segmentation and edge detection is directly beneficial for medical diagnosis. The “proposed 23-layer CNN” architecture is designed to work with a relatively large volume of image data, whereas the “Fine-tuned CNN with VGG16” architecture is designed for a limited amount of image data. A comprehensive data augmentation technique is also conducted to enhance the “Fine-tuned CNN with VGG16” model’s performance. Our experimental results demonstrated that both models enhance the prediction performance of diagnosis of brain tumors. We achieved 97.8% and 100% prediction accuracy for dataset 1 and dataset 2, respectively outperforming previous studies found in the literature. Therefore, we believe that our proposed methods are outstanding candidates for brain tumor detection.

## REFERENCES

Bezdek JC, Hall LO. Review of MR image segmentation techniques using pattern recognition. Med Phys. 1993;20(4):1033–1048.

Deng W, Xiao W. MRI brain tumor segmentation based on improved fuzzy c-means method. In: Proceedings of the Sixth International Symposium on Multispectral Image Processing and Pattern Recognition. International Society for Optics and Photonics; 2009.

Iftikhar A, Iqbal A, Naveed N, Akbar I, Fatima U, Bilal A. An overview of harmful effects of polycystic ovary syndrome. Journal of Oncology Research Review & Reports. 2021;156:2-5.

Asghar I, Ashraf N, Asghar S, Kanwal N, Tanviz F, Bilal A. Deciphering the Regulatory Landscape of the Proteome: A Comprehensive Review of Post-Translational Modifications and Their Implications. Pakistan Journal of Medical & Cardiological Review. 2025 Nov 5;4(4):955-65.

Bilal A. Clinical diagnosis and treatment of absence seizures: Case study. MAR Ophthalmology. 2021;2(1).

Kekre H, Sarode T. Detection of tumor in MRI using vector quantization segmentation. Int J Eng Sci Technol. 2010;2(8):3753–3757.

Logeswari T, Karnan M. An improved implementation of brain tumor detection using segmentation based on soft computing. J Cancer Res Exp Oncol. 2009;2(1):6–14.

Akbar B, Tanvir F, Irfan A, Bilal A, Nawaz A, Minhas H, Basharat M. ANALYSIS OF NON-SYNONYMOUS SNPS IN THE SET ONCOGENE AND THEIR IMPACT ON LEUKEMIA. Journal of Medical & Health Sciences Review. 2025 May 5;2(2).

Mancas M, Gosselin B. Segmentation using a region-growing thresholding. In: Electronic Imaging 2005. International Society for Optics and Photonics; 2005.

Murugavalli S, Rajamani V. An improved implementation of brain tumor detection using segmentation based on neuro-fuzzy technique. 2007;1.

Ahmad RZ, Khan MS, Bilal A, Ali U, Sattar RZ. Effect of locus of control and depression among young adults in Multan (Pakistan). Journal of Asian Development Studies. 2023 Dec 30;12(4):684-92.

Bilal A, Tanvir F, Ahmad S, Shah SH, Ahmad HA, Kanwal N. Pre-clinical study of the bioactive compound Asiaticoside against the proteins inducing human mammary carcinoma using molecular docking and ADME analysis. Remittances Review. 2024 Apr;9(2):3543-76.

Mustaqeem, Javed A. An efficient brain tumor detection algorithm using watershed and thresholding-based segmentation. Int J Image Graph Signal Process. 2012;4(10):34.

Bilal A, Tanvir F, Ahmad S, Kanwal N, Zulfiqar H, Ishaq R. Pharmacokinetic properties of bioactive compounds of aloe vera against pregnancy-associated plasma protein A (PAPP-A) inducing triple-negative breast cancer. Kurdish Studies. 2024 Jun;12(5):157-68.

Padmavathi G, Muthukumar M. Non-linear image segmentation using fuzzy c-means clustering method with thresholding for underwater images. Int J Comput Sci Issues. 2010;7(3):35.

Shahryar M, Umar A, Tanvir F, Zubair F, Rehman S, Sarfraz MZ, Bilal A, Zafar J, Nawaz Y. Gender-Driven UTI Epidemiology and Pan-Resistance Challenges: Cross-Sectional Insights from District Okara Hospitals. Pakistan Journal of Medical & Cardiological Review. 2025 Dec 2;4(4):1397-410.

Jain AK, Mao J, Mohiuddin KM. Neural networks and fuzzy logic applications in pattern recognition. Proc IEEE. 1996;84(2):227–241.

Kumar A, Gupta S, Saxena R. Brain tumor detection from MRI images using segmentation and soft computing techniques. Int J Comput Appl. 2012;49(12):32–39.

Bilal A, Ullah MK, Fatima A, Iqbal K, Khan MS, Nawaz K, Ali U, Qamer SA, Sarfarz A. Epilepsy: A Systematic Review. JOJ Pub Health, 6 (2). 2021.

Pal NR, Pal SK. A review on image segmentation techniques. Pattern Recognit. 2006;26(9):1277–1294.

Bilal A. Impacts of depression on pregnancy: A review. Occupational medicine and health affairs. 2021 Jan 1.

Sezgin M, Sankur B. Survey over image thresholding techniques and quantitative performance evaluation. J Electron Imaging. 2004;13(1):146–165.
Naz S, Hameed IA. Automated techniques for brain tumor segmentation and detection: A review study. In: Proceedings of the 2017 International Conference on Behavioral, Economic, Socio-cultural Computing (BESC); 2017 Oct 16; IEEE. p. 1–6.
Hazra A, Dey A, Gupta SK, Ansari MA. Brain tumor detection based on segmentation using MATLAB. In: Proceedings of the 2017 International Conference on Energy, Communication, Data Analytics and Soft Computing (ICECDS); 2017 Aug 1; IEEE. p. 425–430.
Saini PK, Singh M. Brain tumor detection in medical imaging using MATLAB. Int Res J Eng Technol. 2015;2(2):191–196.
Bilal A, Ansari MS. Prevalence and severity of epilepsy in district Chiniot, Pakistan. Occup Med Health Affairs. 2021;9(3).
Xia Y, Bettinger K, Shen L, Reiss A. Automatic segmentation of the caudate nucleus from human brain MR images. IEEE Trans Med Imaging. 2007;26(4):509–517.
Chu C, Takaya K. Three-dimensional rendering of MR images. In: WESCANEX 93: Communications, Computers and Power in the Modern Environment Conference Proceedings; IEEE; 2003. p. 165–170.
Bilal A, Anjum MI, Naveed N, Saif-ur-Rehman M, Ali U, Iftikhar A. Impacts of abusing drugs on our society. J Med Res Surg. 2021;2(3):1-3.
Clarke LP, Velthuizen RP, Camacho MA, Heine JJ, Vaidyanathan M, Hall LO, et al. MRI segmentation: Methods and applications. Magn Reson Imaging. 2002;13.